Electric-Field-Tunable Edge Transport in Bernal-Stacked Trilayer Graphene

Saurabh Kumar Srivastav,[1,*] Adithi Udupa,[2] K. Watanabe,[3] T. Taniguchi,[3] Diptiman Sen,[2] and Anindya Das[1,†]
[1]Department of Physics, Indian Institute of Science, Bangalore 560012, India
[2]Centre for High Energy Physics, Indian Institute of Science, Bangalore 560012, India
[3]National Institute of Material Science, 1-1 Namiki, Tsukuba 305-0044, Japan

(Received 5 June 2023; revised 29 August 2023; accepted 29 January 2024; published 27 February 2024)

This Letter presents a nonlocal study on the electric-field-tunable edge transport in *h*-BN-encapsulated dual-gated Bernal-stacked (*ABA*) trilayer graphene across various displacement fields (D) and temperatures (T). Our measurements revealed that the nonlocal resistance (R_{NL}) surpassed the expected classical Ohmic contribution by a factor of at least 2 orders of magnitude. Through scaling analysis, we found that the nonlocal resistance scales linearly with the local resistance (R_L) only when the D exceeds a critical value of $\sim$0.2 V/nm. Additionally, we observed that the scaling exponent remains constant at unity for temperatures below the bulk-band gap energy threshold ($T < 25$ K). Further, the value of R_{NL} decreases in a linear fashion as the channel length (L) increases. These experimental findings provide evidence for edge-mediated charge transport in *ABA* trilayer graphene under the influence of a finite displacement field. Furthermore, our theoretical calculations support these results by demonstrating the emergence of dispersive edge modes within the bulk-band gap energy range when a sufficient displacement field is applied.

DOI: 10.1103/PhysRevLett.132.096301

The emergence of gapless edge modes at the physical boundaries of a two-dimensional system is one of the most fascinating phenomena in condensed matter physics. Usually, these edge modes are related to the bulk topological order of the system [1–6] and play a significant role in electronic transport. Some notable examples are the helical edge modes in Z_2 topological insulators [7–10], chiral quantum Hall edge modes [11,12], valley-helical edge modes in graphene [13–17], kink states [13,18], and so on. These edge modes are also believed to be key ingredients for the observation of electric field-induced magnetism [19,20], valley-dependent transport [16,17], and half-metallic behavior in graphene or multilayer graphene [19,20].

Recently, trilayer graphene (TLG) has emerged as a novel two-dimensional material, where several electronic phases, for example, spin-polarized half-metal [21], spin and valley polarized quarter metal [21], superconductivity [22], correlated Chern insulators and ferromagnetism [23], have been realized experimentally. To completely understand the electronic properties of these phases, it is essential to study both bulk and edge transport. Usually, in the absence of a perpendicular displacement field, the band structure of Bernal-stacked TLG is described by a set of linear and quadratic bands, which are similar to the low-energy bands of single and bilayer graphene, respectively, as shown in Fig. 1(b). However, under the application of the large displacement field, the interplay of layer asymmetry and trigonal warping leads to the formation of new sets of Dirac cones, as shown in Fig. 1(c). In addition to modification in the bulk-band structure, the application of displacement field also induces a nontrivial valley Hall state, where the energy gap at the emergent Dirac points is filled by chiral edge modes which propagate in opposite directions between two valleys [24]. Although the emergence of the new sets of the Dirac cones has been experimentally observed in a quantum capacitance measurement [25], an experimental manifestation of the predicted edge modes [24] is still lacking.

Nonlocal transport measurements have been widely used to study the unconventional transport mechanism in two-dimensional systems like the detection of bulk spin and valley transports [26–32]. Along with that, the nonlocal resistance measurement is believed to be an important tool to probe the edge states in the topological insulator [33–35] and has been widely used to explore the edge transport mechanism in several electronic systems [36,37] including the twisted bilayer system [38].

In this work, we have carried out nonlocal resistance measurements in a *h*-BN-encapsulated dual-gated *ABA* TLG device. The measured nonlocal resistance was found to be at least 2 orders of magnitude larger than the classical Ohmic contribution. More importantly, the nonlocal resistance R_{NL} scales linearly with the local resistance R_L, suggesting that the charge transport is edge mediated [34,35,39–42]. The scaling exponent $\alpha(R_{NL} \propto R_L^{\alpha})$ was found to be close to 1 beyond a critical displacement field D. Below the critical field, the edge states are not dispersive and do not contribute significantly to nonlocal transport. Similarly, for temperatures (T) smaller than the

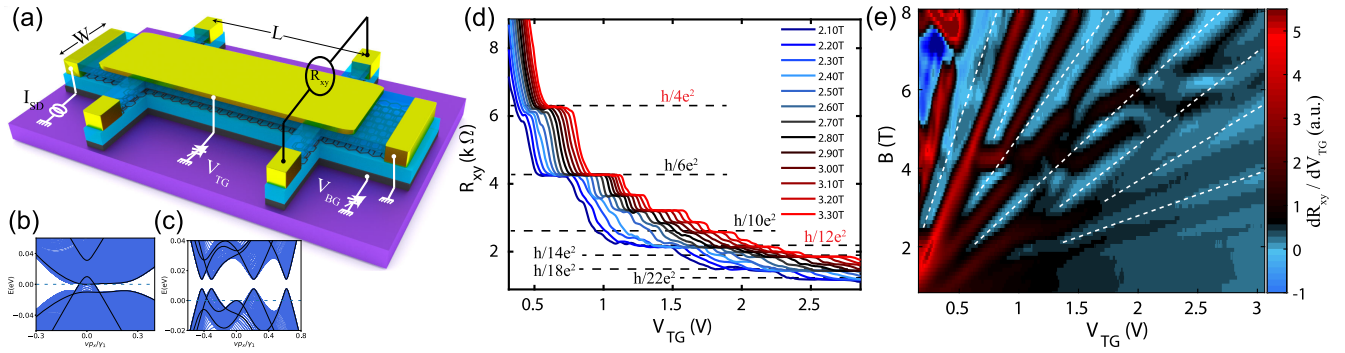

FIG. 1. (a) Schematic of the device configuration: Bernal-stacked trilayer graphene (TLG) is encapsulated between two h-BN substrates and is gated by a graphite back gate (V_{BG}) and a metal top gate (V_{TG}). (b),(c) Band dispersions of Bernal-stacked TLG at zero and finite ($\Delta = 200$ meV) displacement field, respectively. (d) R_{xy} response of the device as a function of V_{TG} for several values of the magnetic field. (e) (dR_{xy}/dV_{TG}) is plotted as a function of V_{TG} and magnetic field. The observation of the crossing points between the different Landau levels, depicted as discontinuities in the QH plateau structure (blue strips) along the white dashed lines, confirms the ABA character of the TLG.

scale of the band gap, α remains close to 1. On further increasing the temperature, α starts deviating from 1 due to the contribution of bulk transport. Moreover, we have measured the R_{NL} at different distances between the injected and measured probes, and found that the value of R_{NL} decreases in a linear fashion as the distance L between the probes increases. This is expected for the edge-mediated transport as described in [42]. To further establish our findings, we perform a theoretical calculation of the edge-mode dispersion for different displacement fields, and found that the edge modes become dispersive only above a critical displacement field, which is consistent with our experimental findings.

For the nonlocal resistance measurement, we fabricated a h-BN-encapsulated Bernal-stacked TLG device using the standard dry transfer technique with a high mobility of $\sim 300\,000$ cm^2 V^{-1} s^{-1}. Our device is gated by a graphite back gate and a metal top gate. The details of the device fabrication are described in the Supplemental Material [43]. Figure 1(a) shows the schematic of the device structure. The electrical resistance was measured using the standard low-frequency lock-in technique. Before discussing details of the nonlocal measurement, we first discuss the quantum Hall response of the device, which establishes the Bernal-stacked trilayer character of the graphene. Figure 1(d) shows a plot of R_{xy} as a function of the top gate voltage V_{TG}. The various color traces correspond to different values of the magnetic field as shown in the legend. One can see that at a low magnetic field, well-developed robust quantum Hall plateaus appear at $h/6e^2, h/10e^2, h/14e^2, \ldots$, which are the characteristic plateaus of TLG [55–59]. We also observe other symmetry broken intermediate plateaus, suggesting the high quality of the device. To further confirm the Bernal-stacked trilayer nature of the graphene, in Fig. 1(e), we plot a two-dimensional color map of dR_{xy}/dV_{TG} as a function of the magnetic field (B) and the top gate voltage V_{TG}. The crossing between the Landau levels of the monolayer and bilayer-like bands, whose energies scale differently with the magnetic field, can be seen as discontinuities in the Quantum Hall (QH) plateau structure (blue strips) along the white dashed lines in Fig. 1(e). The positions of the crossing points are similar to the earlier experimental observations suggesting the ABA character of the TLG [57,60,61].

The dual gate architecture of the device allows us to tune the carrier density n and the displacement field D independently. Figure 2(a) shows a color map of the local resistance (R_L) as a function of the displacement field D and total density n. The resistance at the Dirac point at higher displacement fields does not change significantly, suggesting a small band gap of the ABA TLG consistent with the earlier observations [58,62,63]. Similarly, Fig. 2(b) shows a color map of the nonlocal resistance R_{NL}, (defined as V_{NL}/I) as a function of the displacement field D and total density n. In Fig. 2(c), we plot the line cuts of R_L (red) and R_{NL} (black) as a function of the total density at $D = -0.4$ V/nm. The R_{NL} (black) curve is multiplied by 20 to show it on the same resistance scale axis. To rule out the origin of the Ohmic contribution due to a classical diffusion of charge transport, we calculate the Ohmic contribution using the equation $R_{NL} = (WR_L/\pi L)\exp(-\pi L/W)$, [26,30,31,64,65] with $L = 4$ μm and $W = 1.8$ μm. The measured R_{NL} is 2 orders of magnitude larger than the theoretically calculated Ohmic contribution, suggesting a nontrivial origin of the observed R_{NL}.

Motivated by the earlier nonlocal resistance measurements in the graphene/h-BN superlattice and gapped bilayer graphene devices, we perform a scaling analysis of R_{NL} against R_L. We look for a simple scaling relation $R_{NL} \propto R_L^{\alpha}$ to determine the value of α. We plot $\ln R_{NL}$ versus $\ln R_L$ in Fig. 2(d) as a function of D for different values of n from -3.2 to 5.6×10^{14} m^{-2}, and in Fig. 2(e) as a function of n for different values of D from -0.25 to -0.50 V/nm. The data points for these plots are extracted

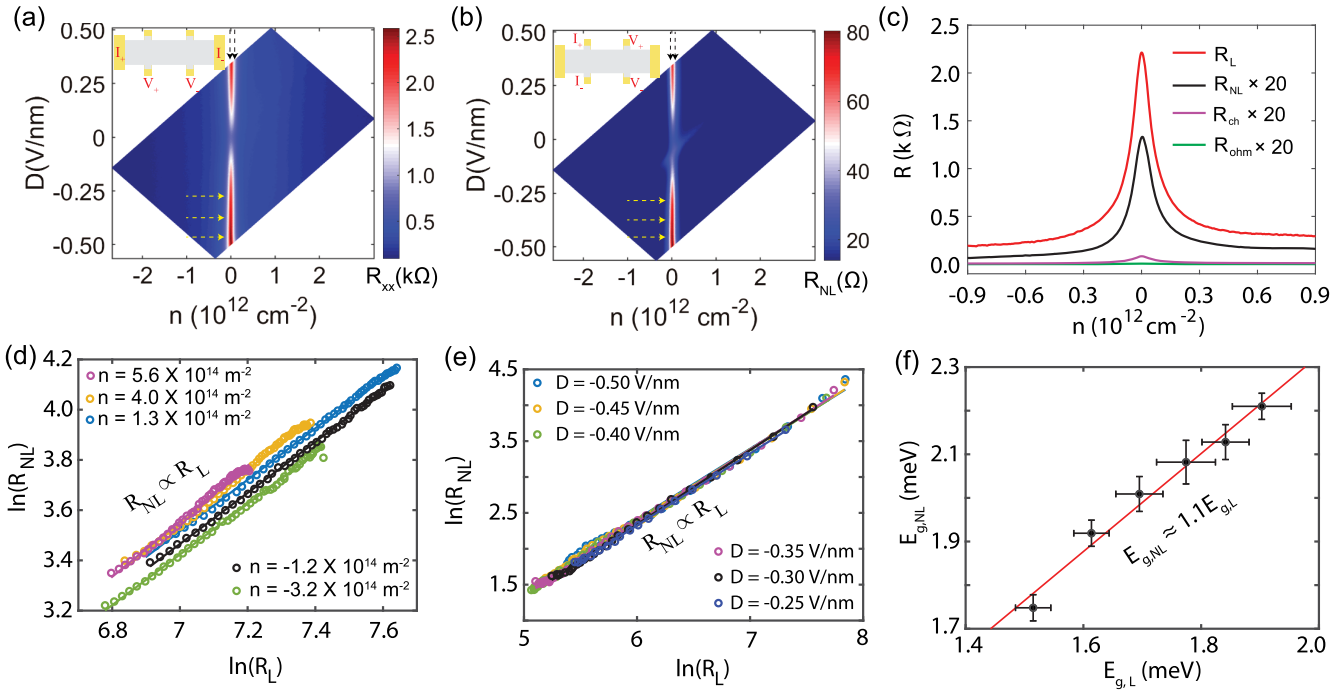

FIG. 2. Color map of R_L (a) and R_{NL} (b) as a function of total carrier density n and the displacement field D. (c) The line cuts of R_L (red) and R_{NL} (black) are plotted with density at $D = -0.4$ V/nm. The R_{NL} is multiplied by a factor of 20. The magenta and green curves (both multiplied by 20) represent the theoretically expected nonlocal contributions from the charge accumulation (near the edge) and classical Ohmic one, respectively. (d),(e) Log-log plots of R_{NL} with R_L. Open circles are extracted from Figs. 2(a) and 2(b) for different values of n (along vertical black arrows) near the Dirac point, (d) and (e), for different values of D (along horizontal yellow arrows). The solid lines correspond to the linear fitting of the data points with slope ~1. (f) The activation gap extracted from R_{NL} is plotted versus the gap extracted from R_L. The red line is the linear fit to these data with slope ~1.1. Different filled circles correspond to the gap extracted at D ranging from −0.29 to −0.50 V/nm. Error bars correspond to the standard deviation associated with the slope of the linear fit.

along the vertical dashed black arrows and the horizontal dashed yellow arrows shown in Figs. 2(a) and 2(b), respectively. The scaling analysis of both Figs. 2(d) and 2(e) shows that linear fitting of the plot $\ln R_{NL}$ versus $\ln R_L$ gives a slope equal to one ($\alpha \approx 1$).

To further investigate the linear scaling of R_{NL} with R_L, we extract the thermal activation gap by measuring the temperature dependence of the local and nonlocal resistances. As shown in figure S6 in [43], R_{NL} also follows an activated behavior at high temperatures similar to the R_L. The temperature dependence of R_L in the activation transport regime is proportional to e^{E_g/k_BT}. If the nonlocal resistance follows the scaling relation $R_{NL} \propto R_L^{\alpha}$, then its temperature dependence will be proportional to $e^{\alpha E_g/k_BT}$. As a result, the activation gap extracted from the nonlocal resistance $(E_{g,NL})$ should be α times of the gap obtained from local resistance $(E_{g,L})$, i.e., $E_{g,NL} = \alpha E_{g,L}$. In Fig. 2(f), we have plotted the activation gap extracted from nonlocal resistance against the gap extracted from local resistance. The filled circles correspond to the gaps extracted at displacement fields ranging from −0.29 to −0.50 V/nm. The red line is the linear fit of these data points with slope ~1.1, again establishing the scaling exponent α close to 1. Note that though the scaling analysis in Fig. 2 is limited (the range of R_L) due to the small band gap opening in *ABA* TLG [as seen in Fig. 2(f)], further scaling analysis for various displacement fields, temperatures, and channel lengths, which will be discussed in the next section, shows that linear scaling is robust for *ABA* TLG.

The linear scaling of R_{NL} with R_L resembles the edge-mediated charge transport by the helical edge modes observed earlier in several two-dimensional electronic systems [34,35,39–41,66]. Thus, we attribute the linear scaling of R_{NL} with R_L to an edge-mediated charge transport in TLG. To strengthen the claim of our findings, we study the effect of the displacement field, temperature, and separation between the probes as described below. It can be seen from Fig. 3(a) that only above a critical $|D| \gtrsim 0.2$ V/nm the α become close to 1. Figure 3(b) shows how α varies with T at $D = -0.45$ V/nm, and it can be seen that $T \gtrsim 25$ K α starts deviating from 1. This is consistent with the edge-mediated charge transport in *ABA* TLG. Above 25 K, which corresponds to an energy scale similar to the band gap opened in *ABA* TLG, the bulk states start contributing to the transport, and α deviates from 1.

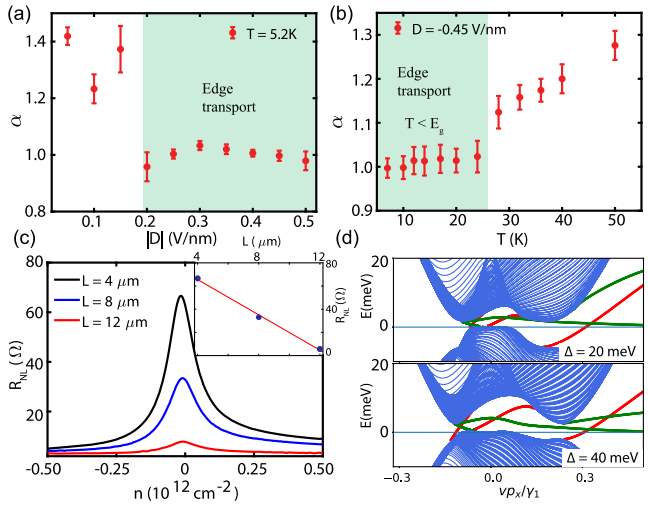

FIG. 3. (a) The scaling exponent α plotted as a function of D at $T = 5.2$ K. For $|D| < 0.2$ V/nm, α deviates significantly from unity. (b) α plotted as a function of T for $D = -0.45$ V/nm. For $T \gtrsim 25$ K α starts deviating from unity. (c) R_{NL} is plotted with density for channel lengths of $L = 4$ μm (black), 8 μm (blue), and 12 μm (red). Inset: The peak value of R_{NL} (blue circles) plotted for different L. The red line is a linear fit. (d) The dispersion of TLG, along with the zigzag edge, is plotted for $\Delta = 20$ meV (top) and $\Delta = 40$ meV (bottom). The green (red) curves correspond to modes on the right (left) edge of the system.

Figure 3(c) shows R_{NL} for different L, and it can be seen from the inset that R_{NL} decreases linearly with L, which is in accordance with edge-mediated transport as reported for the quantum spin Hall phase and topological insulators [34,35,39–42]. Note that similar results (critical D) are obtained for positive displacement fields. However, due to the limited range of D on the positive side, as seen in Fig. 2(b), we have presented the data for negative D. We have repeated the experiment in different thermal cycles, which is summarized in Sec. 8 in [43], and it shows similar results with scaling exponent 1.

To understand edge-mediated nonlocal charge transport, we now perform theoretical calculations to confirm the presence of edge states in TLG in the presence of the desired displacement field. We consider a potential drop of 2Δ between the top and bottom layer of TLG due to applying the external displacement field. The magnitude Δ is related to the experimentally applied displacement field D via the relation $2\Delta = -[(d_\perp/\epsilon_{\mathrm{TLG}}) \times D]e$, where $d_\perp = 0.67$ nm is the separation between the top and bottom layers of TLG, ϵ_{TLG} is the dielectric constant of the TLG, and e is the electronic charge. Considering the electric field, the Hamiltonian for this system has a form described in detail in [43]. The presence of Δ opens up a gap in the bulk dispersion but, more interestingly, also gives rise to six new Dirac points each around the Dirac points K and K'. These play a major role in hosting the edge states in this system.

The Hamiltonian is time-reversal symmetric, implying that the total Hall conductivity σ_{xy} summed over all the valleys must be zero. But if we look at a particular valley, the system has a nonzero σ^V_{xy}. We estimate this quantity by numerically calculating the valley Chern number using the method of Fukui *et al.* [67] in the discretized Brillouin zone close to a Dirac point (see [43] for details). Although the total Chern number summed over valleys is zero, the valley Chern number C^V equals 2.5 for all the values of Δ relevant to the corresponding experimental values of D. This implies that there is a nonzero valley Hall conductivity of $\sigma^V_{xy} = -2.5(e^2/\hbar)$, which agrees with the theoretically predicted value in Ref. [24]. The nonzero valley Chern number suggests that there is a possibility of having edge modes in the system. However, the edge modes would not be robust to perturbations since the counterpropagating modes from K and K' valley can hybridize.

In TLG, for Δ from 20 meV to 50 meV, we find that for a zig-zag edge configuration, the edges host gapless modes in the bulk gap. The method used for determining these edge modes is given in [43]. Figure 3(d) shows plots for $\Delta = 20$ meV and $\Delta = 40$ meV with the edge modes in green (red) for the right (left) edge of the system. Since they are present in the bulk gap, they participate in transport along the edges. However, we note that these edge modes are not protected from backscattering. Hence, there can be intervalley scattering between the states, and a simple dissipative model for edge transport can mimic this and explain the linear scaling between local and nonlocal resistances as described using a resistor network circuit model in Ref. [42]. Further, the circuit model (equation S20 of Ref. [42]) as explained in Sec. 4 in [43] captures linear decay of the nonlocal resistance with the channel length (L) as seen in our experiment [the inset of Fig. 3(c)]. We would like to point out that this is unlike the experimental results for bilayer graphene [42], where the bulk valley Hall effect dominates and gives a cubic relation between R_{NL} and R_L as reported in Refs. [31 and [42]. From our theoretical calculation, we also find that for small values of the displacement field below 20 meV (see Fig. S10 in [43]), the edge modes are approximately flat and nondispersive, thus not contributing to the nonlocal charge transport significantly. This is consistent with the experimental results, where we find that as a function of the displacement field, α deviates from one for values of $|D|$ below 0.15 V/nm ($\Delta < 20$ meV) as shown in Fig. 3(b). This is also consistent with Zibrov *et al.* [25], where at the similar displacement field, the Fermi surface undergoes a Lifshitz transition from one electron pocket to multiple isolated Dirac cones.

In general, the nonlocal signal can originate from mainly three different sources: (i) classical contribution, (ii) a new kind of topological effect—bulk valley Hall effect [30,31,42], or (iii) edge transport due to either topological [24,68,69] or nontopological (charge accumulation) [70]

edge modes. These three mechanisms have also been highlighted in Refs. [71,72]. Although the nonlocal measurement is not a smoking gun to distinguish its origin, estimating the nonlocal contributions from the different sources can help to find its dominant contribution. As shown in Fig. 2(c) by the green solid line, the classical Ohmic one is ruled out, and similarly, as mentioned before, the linear scaling between R_{NL} with R_L in specific parameter spaces of temperature and displacement field, rule out the bulk valley Hall effect. Now, the question is whether the observed edge transport in our experiment originated from a topological or nontopological effect. To figure it out, we estimate the contribution from the nontopological charge accumulation effect (R_{ch}) [70], which is shown by the solid magenta line in Fig. 2(c) (detail in Sec. 7 in [43]), which is one order of magnitude smaller than the measured nonlocal signal [solid black line in Fig. 2(c)]. Further, the linear decay of R_{NL} with L [Fig. 3(c)] rules out the charge accumulation contribution, which would have scaled exponentially with the length [70] (see Sec. 7 in [43]). Thus, the dominant contribution to our nonlocal signal presumably comes from the dispersive edge modes of TLG as predicted in Ref. [24] and shown by our theoretical calculation (beyond a critical displacement field). Our findings are in sharp contrast to Ref. [70] on a nonaligned single-layer graphene device, where the dominant contribution to the nonlocal signal was the charge accumulation effect [70], and is expected due to the absence of dispersive edge modes [73].

In conclusion, the consistent linear scaling of nonlocal resistance across temperature variations, displacement field changes, and a threefold variation in channel length corresponds to the dispersive edge mode transport in correlation with our theoretical calculations.

S. K. S. thanks Adhip Agarwala, Priya Tiwari, and Manbendra Kuiri, for useful discussions. S. K. S. acknowledges Prime Minister Research Fellowship, Ministry of Education, India for financial support. D. S. thanks SERB, India for support through Project No. JBR/2020/000043. A. D. thanks the Department of Science and Technology (DST) and Science and Engineering Research Board (SERB), India for financial support (SP/SERB-22-0387) and acknowledges the Swarnajayanti Fellowship of the DST/SJF/PSA-03/2018-19. A. D. also thanks CEFIPRA Project No. SP/IFCP-22-0005.

*Corresponding author: ssaurabh@iisc.ac.in
†Corresponding author: anindya@iisc.ac.in

[1] D. J. Thouless, M. Kohmoto, M. P. Nightingale, and M. den Nijs, Quantized Hall conductance in a two-dimensional periodic potential, Phys. Rev. Lett. **49**, 405 (1982).
[2] Y. Hatsugai, Chern number and edge states in the integer quantum Hall effect, Phys. Rev. Lett. **71**, 3697 (1993).
[3] X.-L. Qi, Y.-S. Wu, and S.-C. Zhang, General theorem relating the bulk topological number to edge states in two-dimensional insulators, Phys. Rev. B **74**, 045125 (2006).
[4] C. L. Kane and E. J. Mele, Z_2 topological order and the quantum spin Hall effect, Phys. Rev. Lett. **95**, 146802 (2005).
[5] L. Fu and C. L. Kane, Time reversal polarization and a z_2 adiabatic spin pump, Phys. Rev. B **74**, 195312 (2006).
[6] J. E. Moore and L. Balents, Topological invariants of time-reversal-invariant band structures, Phys. Rev. B **75**, 121306(R) (2007).
[7] C. L. Kane and E. J. Mele, Quantum spin Hall effect in graphene, Phys. Rev. Lett. **95**, 226801 (2005).
[8] B. A. Bernevig and S.-C. Zhang, Quantum spin Hall effect, Phys. Rev. Lett. **96**, 106802 (2006).
[9] B. A. Bernevig, T. L. Hughes, and S.-C. Zhang, Quantum spin Hall effect and topological phase transition in HgTe quantum wells, Science **314**, 1757 (2006).
[10] M. Onoda and N. Nagaosa, Spin current and accumulation generated by the spin Hall insulator, Phys. Rev. Lett. **95**, 106601 (2005).
[11] R. B. Laughlin, Quantized Hall conductivity in two dimensions, Phys. Rev. B **23**, 5632 (1981).
[12] B. I. Halperin, Quantized Hall conductance, current-carrying edge states, and the existence of extended states in a two-dimensional disordered potential, Phys. Rev. B **25**, 2185 (1982).
[13] I. Martin, Y. M. Blanter, and A. F. Morpurgo, Topological confinement in bilayer graphene, Phys. Rev. Lett. **100**, 036804 (2008).
[14] Z. Qiao, J. Jung, Q. Niu, and A. H. MacDonald, Electronic highways in bilayer graphene, Nano Lett. **11**, 3453 (2011).
[15] F. Zhang, A. H. MacDonald, and E. J. Mele, Valley Chern numbers and boundary modes in gapped bilayer graphene, Proc. Natl. Acad. Sci. U.S.A. **110**, 10546 (2013).
[16] J. Li, K. Wang, K. J. McFaul, Z. Zern, Y. Ren, K. Watanabe, T. Taniguchi, Z. Qiao, and J. Zhu, Gate-controlled topological conducting channels in bilayer graphene, Nat. Nanotechnol. **11**, 1060 (2016).
[17] J. Li, R.-X. Zhang, Z. Yin, J. Zhang, K. Watanabe, T. Taniguchi, C. Liu, and J. Zhu, A valley valve and electron beam splitter, Science **362**, 1149 (2018).
[18] J. Jung, F. Zhang, Z. Qiao, and A. H. MacDonald, Valley-Hall kink and edge states in multilayer graphene, Phys. Rev. B **84**, 075418 (2011).
[19] Y.-W. Son, M. L. Cohen, and S. G. Louie, Half-metallic graphene nanoribbons, Nature (London) **444**, 347 (2006).
[20] Y.-W. Son, M. L. Cohen, and S. G. Louie, Energy gaps in graphene nanoribbons, Phys. Rev. Lett. **97**, 216803 (2006).
[21] H. Zhou, T. Xie, A. Ghazaryan, T. Holder, J. R. Ehrets, E. M. Spanton, T. Taniguchi, K. Watanabe, E. Berg, M. Serbyn *et al.*, Half-and quarter-metals in rhombohedral trilayer graphene, Nature (London) **598**, 429 (2021).
[22] H. Zhou, T. Xie, T. Taniguchi, K. Watanabe, and A. F. Young, Superconductivity in rhombohedral trilayer graphene, Nature (London) **598**, 434 (2021).
[23] G. Chen, A. L. Sharpe, E. J. Fox, Y.-H. Zhang, S. Wang, L. Jiang, B. Lyu, H. Li, K. Watanabe, T. Taniguchi *et al.*, Tunable correlated Chern insulator and ferromagnetism in a moiré superlattice, Nature (London) **579**, 56 (2020).

[24] T. Morimoto and M. Koshino, Gate-induced Dirac cones in multilayer graphenes, Phys. Rev. B **87**, 085424 (2013).
[25] A. A. Zibrov, P. Rao, C. Kometter, E. M. Spanton, J. I. A. Li, C. R. Dean, T. Taniguchi, K. Watanabe, M. Serbyn, and A. F. Young, Emergent Dirac gullies and gully-symmetry-breaking quantum Hall states in *aba* trilayer graphene, Phys. Rev. Lett. **121**, 167601 (2018).
[26] J. Balakrishnan, G. Kok Wai Koon, M. Jaiswal, A. Castro Neto, and B. Özyilmaz, Colossal enhancement of spin–orbit coupling in weakly hydrogenated graphene, Nat. Phys. **9**, 284 (2013).
[27] J. Balakrishnan, G. K. W. Koon, A. Avsar, Y. Ho, J. H. Lee, M. Jaiswal, S.-J. Baeck, J.-H. Ahn, A. Ferreira, M. A. Cazalilla *et al.*, Giant spin Hall effect in graphene grown by chemical vapour deposition, Nat. Commun. **5**, 4748 (2014).
[28] Y. Wang, X. Cai, J. Reutt-Robey, and M. S. Fuhrer, Neutral-current Hall effects in disordered graphene, Phys. Rev. B **92**, 161411(R) (2015).
[29] A. A. Kaverzin and B. J. van Wees, Electron transport nonlocality in monolayer graphene modified with hydrogen silsesquioxane polymerization, Phys. Rev. B **91**, 165412 (2015).
[30] R. Gorbachev, J. Song, G. Yu, A. Kretinin, F. Withers, Y. Cao, A. Mishchenko, I. Grigorieva, K. S. Novoselov, L. Levitov *et al.*, Detecting topological currents in graphene superlattices, Science **346**, 448 (2014).
[31] M. Sui, G. Chen, L. Ma, W.-Y. Shan, D. Tian, K. Watanabe, T. Taniguchi, X. Jin, W. Yao, D. Xiao *et al.*, Gate-tunable topological valley transport in bilayer graphene, Nat. Phys. **11**, 1027 (2015).
[32] J. Pan, T. Zhang, H. Zhang, B. Zhang, Z. Dong, and P. Sheng, Berry curvature and nonlocal transport characteristics of antidot graphene, Phys. Rev. X **7**, 031043 (2017).
[33] A. P. Protogenov, V. A. Verbus, and E. V. Chulkov, Nonlocal edge state transport in topological insulators, Phys. Rev. B **88**, 195431 (2013).
[34] G. M. Gusev, Z. D. Kvon, O. A. Shegai, N. N. Mikhailov, S. A. Dvoretsky, and J. C. Portal, Transport in disordered two-dimensional topological insulators, Phys. Rev. B **84**, 121302(R) (2011).
[35] I. Knez, C. T. Rettner, S.-H. Yang, S. S. P. Parkin, L. Du, R.-R. Du, and G. Sullivan, Observation of edge transport in the disordered regime of topologically insulating InAs/GaSb quantum wells, Phys. Rev. Lett. **112**, 026602 (2014).
[36] A. Roth, C. Brüne, H. Buhmann, L. W. Molenkamp, J. Maciejko, X.-L. Qi, and S.-C. Zhang, Nonlocal transport in the quantum spin Hall state, Science **325**, 294 (2009).
[37] Z. Fei, T. Palomaki, S. Wu, W. Zhao, X. Cai, B. Sun, P. Nguyen, J. Finney, X. Xu, and D. H. Cobden, Edge conduction in monolayer WTe_2, Nat. Phys. **13**, 677 (2017).
[38] Y. Wang, J. Herzog-Arbeitman, G. W. Burg, J. Zhu, K. Watanabe, T. Taniguchi, A. H. MacDonald, B. A. Bernevig, and E. Tutuc, Bulk and edge properties of twisted double bilayer graphene, Nat. Phys. **18**, 48 (2022).
[39] F. Nichele, A. N. Pal, P. Pietsch, T. Ihn, K. Ensslin, C. Charpentier, and W. Wegscheider, Insulating state and giant nonlocal response in an InAs/GaSb quantum well in the quantum Hall regime, Phys. Rev. Lett. **112**, 036802 (2014).
[40] L. Du, I. Knez, G. Sullivan, and R.-R. Du, Robust helical edge transport in gated InAs/GaSb bilayers, Phys. Rev. Lett. **114**, 096802 (2015).
[41] I. Knez, R.-R. Du, and G. Sullivan, Evidence for helical edge modes in inverted InAs/GaSb quantum wells, Phys. Rev. Lett. **107**, 136603 (2011).
[42] Y. Shimazaki, M. Yamamoto, I. V. Borzenets, K. Watanabe, T. Taniguchi, and S. Tarucha, Generation and detection of pure valley current by electrically induced Berry curvature in bilayer graphene, Nat. Phys. **11**, 1032 (2015).
[43] See Supplemental Material at http://link.aps.org/supplemental/10.1103/PhysRevLett.132.096301 for details of sample characterization, measurements, additional data, and theoretical analysis, which includes Refs. [44–54].
[44] L. Wang, I. Meric, P. Huang, Q. Gao, Y. Gao, H. Tran, T. Taniguchi, K. Watanabe, L. Campos, D. Muller *et al.*, One-dimensional electrical contact to a two-dimensional material, Science **342**, 614 (2013).
[45] L. Malard, M. A. Pimenta, G. Dresselhaus, and M. Dresselhaus, Raman spectroscopy in graphene, Phys. Rep. **473**, 51 (2009).
[46] C. H. Lui, Z. Li, Z. Chen, P. V. Klimov, L. E. Brus, and T. F. Heinz, Imaging stacking order in few-layer graphene, Nano Lett. **11**, 164 (2011).
[47] C. Cong, T. Yu, K. Sato, J. Shang, R. Saito, G. F. Dresselhaus, and M. S. Dresselhaus, Raman characterization of ABA-and ABC-stacked trilayer graphene, ACS Nano **5**, 8760 (2011).
[48] A. Venugopal, J. Chan, X. Li, C. W. Magnuson, W. P. Kirk, L. Colombo, R. S. Ruoff, and E. M. Vogel, Effective mobility of single-layer graphene transistors as a function of channel dimensions, J. Appl. Phys. **109**, 104511 (2011).
[49] C. Kumar, S. K. Srivastav, P. Adhikary, S. Banerjee, T. Das, and A. Das, Localization physics in graphene moiré superlattices, Phys. Rev. B **98**, 155408 (2018).
[50] C. Kumar, S. K. Srivastav, and A. Das, Equilibration of quantum Hall edges in symmetry-broken bilayer graphene, Phys. Rev. B **98**, 155421 (2018).
[51] M. Kuiri, S. K. Srivastav, S. Ray, K. Watanabe, T. Taniguchi, T. Das, and A. Das, Enhanced electron-phonon coupling in doubly aligned hexagonal boron nitride bilayer graphene heterostructure, Phys. Rev. B **103**, 115419 (2021).
[52] P. Tiwari, S. K. Srivastav, and A. Bid, Electric-field-tunable valley zeeman effect in bilayer graphene heterostructures: Realization of the spin-orbit valve effect, Phys. Rev. Lett. **126**, 096801 (2021).
[53] J. Renard, M. Studer, and J. A. Folk, Origins of nonlocality near the neutrality point in graphene, Phys. Rev. Lett. **112**, 116601 (2014).
[54] G. Kirczenow, Valley currents and nonlocal resistances of graphene nanostructures with broken inversion symmetry from the perspective of scattering theory, Phys. Rev. B **92**, 125425 (2015).
[55] M. Ezawa, Supersymmetry and unconventional quantum hall effect in monolayer, bilayer and trilayer graphene, Physica (Amsterdam) **40E**, 269 (2007).
[56] M. Koshino and E. McCann, Parity and valley degeneracy in multilayer graphene, Phys. Rev. B **81**, 115315 (2010).
[57] T. Taychatanapat, K. Watanabe, T. Taniguchi, and P. Jarillo-Herrero, Quantum Hall effect and Landau-level crossing of

Dirac fermions in trilayer graphene, Nat. Phys. **7**, 621 (2011).
[58] E. A. Henriksen, D. Nandi, and J. P. Eisenstein, Quantum Hall effect and semimetallic behavior of dual-gated ABA-stacked trilayer graphene, Phys. Rev. X **2**, 011004 (2012).
[59] S. Yuan, R. Roldán, and M. I. Katsnelson, Landau level spectrum of ABA-and ABC-stacked trilayer graphene, Phys. Rev. B **84**, 125455 (2011).
[60] L. C. Campos, T. Taychatanapat, M. Serbyn, K. Surakitbovorn, K. Watanabe, T. Taniguchi, D. A. Abanin, and P. Jarillo-Herrero, Landau level splittings, phase transitions, and nonuniform charge distribution in trilayer graphene, Phys. Rev. Lett. **117**, 066601 (2016).
[61] B. Datta, S. Dey, A. Samanta, H. Agarwal, A. Borah, K. Watanabe, T. Taniguchi, R. Sensarma, and M. M. Deshmukh, Strong electronic interaction and multiple quantum Hall ferromagnetic phases in trilayer graphene, Nat. Commun. **8**, 14518 (2017).
[62] B. Datta, H. Agarwal, A. Samanta, A. Ratnakar, K. Watanabe, T. Taniguchi, R. Sensarma, and M. M. Deshmukh, Landau level diagram and the continuous rotational symmetry breaking in trilayer graphene, Phys. Rev. Lett. **121**, 056801 (2018).
[63] M. Koshino and E. McCann, Gate-induced interlayer asymmetry in ABA-stacked trilayer graphene, Phys. Rev. B **79**, 125443 (2009).
[64] C. Brüne, A. Roth, E. Novik, M. König, H. Buhmann, E. Hankiewicz, W. Hanke, J. Sinova, and L. Molenkamp, Evidence for the ballistic intrinsic spin Hall effect in HgTe nanostructures, Nat. Phys. **6**, 448 (2010).
[65] D. Abanin, S. Morozov, L. Ponomarenko, R. Gorbachev, A. Mayorov, M. Katsnelson, K. Watanabe, T. Taniguchi, K. Novoselov, L. Levitov *et al.*, Giant nonlocality near the Dirac point in graphene, Science **332**, 328 (2011).
[66] P. Tiwari, S. K. Srivastav, S. Ray, T. Das, and A. Bid, Observation of time-reversal invariant helical edge-modes in bilayer graphene/WSe_2 heterostructure, ACS Nano **15**, 916 (2020).
[67] T. Fukui, Y. Hatsugai, and H. Suzuki, Chern numbers in discretized brillouin zone: Efficient method of computing (spin) Hall conductance, J. Phys. Soc. Jpn. **74**, 1674 (2005).
[68] R. Brown, N. R. Walet, and F. Guinea, Edge modes and nonlocal conductance in graphene superlattices, Phys. Rev. Lett. **120**, 026802 (2018).
[69] J. Marmolejo-Tejada, J. H. Garcia, M. Petrović, P. Chang, X. Sheng, A. Cresti, P. Plecháč, S. Roche, and B. Nikolić, Deciphering the origin of nonlocal resistance in multi-terminal graphene on hexagonal-boron-nitride with *ab initio* quantum transport: fermi surface edge currents rather than Fermi sea topological valley currents, J. Phys. **1**, 015006 (2018).
[70] A. Aharon-Steinberg, A. Marguerite, D. J. Perello, K. Bagani, T. Holder, Y. Myasoedov, L. S. Levitov, A. K. Geim, and E. Zeldov, Long-range nontopological edge currents in charge-neutral graphene, Nature (London) **593**, 528 (2021).
[71] S. Roche, S. R. Power, B. K. Nikolić, J. H. García, and A.-P. Jauho, Have mysterious topological valley currents been observed in graphene superlattices?, J. Phys. **5**, 021001 (2022).
[72] L. F. Torres and S. O. Valenzuela, A valley of opportunities, Phys. World **34**, 43 (2021).
[73] K. Nakada, M. Fujita, G. Dresselhaus, and M. S. Dresselhaus, Edge state in graphene ribbons: Nanometer size effect and edge shape dependence, Phys. Rev. B **54**, 17954 (1996).